TISSUE ENGINEERING: Part A
Volume 20, Numbers 13 and 14, 2014

DOI: 10.1089/ten.tea.2013.0352

A Combination of Biphasic Calcium Phosphate Scaffold with Hyaluronic Acid-Gelatin Hydrogel as a New Tool for Bone Regeneration

Thuy Ba Linh Nguyen, PhD,[1,2] and Byong-Taek Lee, PhD[1,2]

A novel bone substitute was fabricated to enhance bone healing by combining ceramic and polymer materials. In this study, Hyaluronic acid (HyA)–Gelatin (Gel) hydrogel was loaded into a biphasic calcium phosphate (BCP) ceramic, and the resulting scaffold, with unique micro- and macroporous orientation, was evaluated for bone regeneration applications. The fabricated scaffold showed high interconnected porosity, with an average compressive strength of 2.8 ± 0.15 MPa, which is usually recommended for cancellous bone substitution. *In vitro* cytocompatibility studies were conducted using bone marrow mesenchymal stem cells. The HyA-Gel–loaded BCP scaffold resulted in a significant increase in cell proliferation at 3 ($p < 0.05$) and 7 days ($p < 0.001$) and high alkaline phosphatase activities at 14 and 21 days. Furthermore, the *in vivo* studies showed that the implanted HyA-Gel–loaded BCP scaffold begins to degrade within 3 months after implantation. Histological sections also confirmed a rapid new bone formation and a high rate of collagen mineralization. A bone matrix formation was confirmed by positive immunohistochemistry staining of osteopontin, osteocalcin, and collagen type I. *In vivo* expression of extracellular matrix proteins demonstrated that this novel bone substitute holds great promise for use in stimulating new bone regeneration.

Introduction

Repair of fractured or diseased bone requires an initial structural support, as well as the development and organization of bone tissues, which can be achieved by designing appropriate internal scaffolds.[1–5] Composites of biopolymers and bioceramics are currently being developed with the goals of increasing the mechanical stability of the bone substitute and improving tissue–scaffold interactions.[6] Biphasic calcium phosphate (BCP), which consists of hydroxyapatite (HAp) and tricalcium phosphate (TCP) phases, is considered to be a more efficient ceramic material and an ideal bone substitute, due to its controllable degradability and favorable biological properties, such as having a high bioresorption rate.[7–8] In the present study, a sponge BCP scaffold was fabricated using a sponge replica method, and a porous hyaluronic acid (HyA)–gelatin (Gel) hydrogel was loaded into a three-dimensional (3D) ceramic sponge, followed by freeze drying to facilitate macro- and microporous orientation in the architecture, as well as to improve the cell attachment and supports to guide the cellular functionality of the final scaffold. Hydrogels temporarily play the role of an extracellular matrix (ECM) during the early regenerative stage.[9] As tissue formation progresses, the hydrogel matrices are replaced by a natural ECM. Hydrogels are 3D networks capable of absorbing a large amount of water, allowing for the diffusion of nutrients and metabolites from the cells. HyA is a nonsulfated glucosaminoglycan, which is produced by hyaluron synthase at the plasma membrane of cells.[10] In addition, HyA has been shown to have strong effects on cell motility and cell–cell interactions.[11–13] Gelatin is formed by breaking the natural triple helix structure of a collagen into single-strand molecules through hydrolysis. Gelatin has been used previously to promote cell adhesion, migration, differentiation, and proliferation in tissue engineering.[14–16]

In this study, we studied and developed a novel hybrid system in a cohort of a series of *in vitro* experiments with bone marrow mesenchymal stem cells (BMSCs), and then implanted the novel substitute to demonstrate its functionality *in vivo*.

Materials and Methods

Process for fabricating porous scaffolds

Porous HyA-Gel scaffold preparation. Hyaluronic acid sodium salt (HyA) was purchased from Fluka, gelatin type A from porcine skin (Gel), and 1-ethyl-3(3-dimethylaminopropyl), carbodiimide hydrochloride (EDAC), and N-hydroxyl succinimide (NHS) were purchased from Sigma Chemical Co. Gel

[1]Department of Regenerative Medicine and [2]Institute of Tissue Regeneration, College of Medicine, Soonchunhyang University, Cheonan, South Korea.

(10 wt%, 300 Bloom) was dissolved in deionized (DI)[17] water at 30°C. Adequate amounts of HyA (0.5 wt%) were added to the Gel solution until it became a slurry at a volume ratio of 15:85 (HyA:Gel).[18] The slurry was frozen at −80°C for 8 h and was then lyophilized at −70°C overnight to prepare the porous scaffold. The porous scaffolds were crosslinked using EDAC and NHS at a 5:2 molar ratio in 80% ethanol overnight at 4°C.

Porous HyA-Gel/BCP scaffolds. The BCP scaffold was fabricated using the sponge replica method from our previous study.[19] Briefly, the polyurethane sponge (60 ppi, HD sponge) was immersed in a BCP slurry containing 5% PVB and 10% BCP powder. The final scaffolds were sintered in a microwave furnace (UMF-01, 2.45 GHz; Unicera) at 1200°C for 10 min with a heating rate of 100°C/min.

The sponge BCP scaffolds were washed in distilled water under ultrasonication and dried to remove the contaminate inside the sponge scaffolds. The HyA-Gel solution was placed in a syringe and passed through a filter that was connected to a vacumn container. The sponge BCP was placed inside the container. To prepare the hydrid sponges of BCP and HyA-Gel hydrogel, the HyA-Gel solution was added dropwise into the sponge BCP scaffolds under vacumn, so that the spongy pores of BCP filled with the HyA-Gel solution. The scaffolds were frozen at −80°C for 8 h, and freeze-dried for 48 h at −80°C to completely remove the DI water. The scaffolds containing the HyA-Gel hydrogel in sponge BCP were crosslinked with the EDAC solution (as mentioned above), washed with DI water, and freeze-dried to form the hybrid sponge HyA-Gel in sponge BCP (HyA-Gel/BCP).

Structural and chemical analysis of the scaffolds

An inverted light microscope (Olympus; 1×71) and a scanning electron microscope (SEM, JEOL, JSM-6701F) were used to observe the morphology of the sponge BCP, HyA-Gel, and HyA-Gel/BCP scaffolds. An energy dispersive X-ray spectrometer (EDS, JSM-7401F) equipped with SEM was used to analyze the element composition of the HyA-Gel/BCP scaffold.

The crystal structures of the BCP, HyA-Gel, and HyA-Gel/BCP scaffolds were subjected to X-ray diffraction (XRD) (Rigaku, D/MAX—2500 V) using CuK_α radiation generated at 40 kV and 200 mA. The diffraction angle varied from 10 to 60 2θ.

A mercury porosimeter (PoreMaster™; Quantachrome Instruments) was used to analyze the porosity and pore size distribution of the scaffolds.[12] The scaffolds with dimensions of width × length × height = 5 × 7 × 7 mm were placed in a penetrometer and infused with mercury under increasing pressure.

Compressive strength was determined using a universal testing machine (R&B UNITECH-T). The samples were prepared in another polyethylene mold with dimensions of width × length × height = 5 × 7 × 7 mm. The measurements were taken using a 1 kN load cell. Load deformation data were recorded at a deforming speed of 0.5 mm/s.

In vitro *cytocompatibility*

Isolation and cultivation of rabbit BMSCs. BMSC aspirates were isolated from the bone shafts of femurs from 2-week-old New Zealand white rabbits (Samtako Bio Korea).[20–22] The bone marrow aspirates were filtered by using a cell strainer filter (100 μm nylon; Falcon), pooled, and centrifuged for 5 min at 1500 rpm to remove the supernatants. The cell pellet was resuspended in the α-MEM (MEM; HyClone) with 10% fetal bovine serum (FBS) and 1% penicillin/streptomycin (antibiotics). To count the cells, a small aliquot of cells was suspended in 5% acetic acid to remove the red blood cells, and mononuclear cells were counted by trypan blue exclusion. After counting, 1.0×10^7 cells were seeded in a culture dish (ϕ 150) and were cultured for 10–14 days as a monolayer in a humidified incubator at 37°C in an atmosphere of 5% CO_2 (incubator; ASTEC). Third passage cells were used in subsequent cultures.

Cell proliferation and viability assay. Approximately 10^4 BMSCs/mL were seeded on the top of the BCP, HyA-Gel, and HyA-Gel/BCP scaffolds. For observation by the confocal microscope (Olympus FV 10i), after 1, 3, 7, and 14 days of culture, the scaffolds were immunostained using fluorescein isothiocyanate (FITC)-conjugated phalloidin (25 μg/mL-Sigma).[18,23] Nuclei were counterstained with 4′, 6′-diamidino-2-phenylindole (DAPI). Finally, the scaffolds were mounted onto glass slides and were visualized under a confocal fluorescent microscope using 10× and 60× objectives and the accompanying FV10i-ASW 3.0 Viewer software.

The MTT (3-[4, 5-dimethylthiazol-2-yl]-2, 5-diphenyltetrazolium bromide) assay[24] was used to analyze cell viability. A 10^4 cell/mL of media was seeded onto the surface of the test materials and control materials (cultured media only). The cell viability (OD) at 1, 3, and 7 days on the scaffold was quantified by adding 100 μL of MTT solution (5 mg/mL in PBS) to each well of a 24-well tissue culture plate. The OD values of the solution were measured using an ELISA reader (EL, 312, Biokinetics reader; Bio-Tek instruments) at a wavelength of 595 nm.

Osteogenic differentiation. The osteogenic differentiation of BMSCs was analyzed by ALP staining (Alkaline Phosphate Staining Kit-PMC-AK20-COS) and immunocytochemical analysis on days 14 and 21.

Immunocytochemical analysis of osteopontin (OPN) and osteocalcin (OCN) (bone-specific protein) was performed by incubating the scaffolds with the mouse anti-OPN antibody (1:200, NB110-89062; Novus Biologicals) and the mouse anti-OCN antibody (1:200, ab13418; abcam) overnight at 4°C. Then, the scaffolds were incubated in the anti-mouse secondary antibody (Alexa flour 488, 1:1000; Invitrogen). The images were visualized under a confocal fluorescent microscope (FV10i-W) using 10× objectives and the accompanying FV10i-ASW 3.0 Viewer software.

In vivo *biocompatibility*

Animals and surgical procedure. New Zealand white rabbits (weight 3 kg) were purchased commercially, caged in different stainless steel housing facilities, and approved food and water were supplied properly according to the guidelines provided by the Animal Care Center, SoonchunHyang University, Chungcheongnam-do, South Korea. An acclimation period was provided to adjust the environment before the operation day, and all rabbits were anesthetized before the operation. Hair on the femur was thoroughly shaved and sterilized with 70% ethanol and the area was cleaned with iodine. An incision was made on the parietal part of the

femur, and a 4×5 mm hole was drilled in the right-hand side of the sagittal border using a trephine drill, with continuous saline washing to prevent tissue dehydration. The HyA-Gel/BCP scaffolds were placed over the drilled parietal bone after sterilization and sterile saline washing. The subcutaneous tissue was closed, and the overlying skin was resutured. Laboratory animals were kept and fed *ad libitum.*

The rabbits were sacrificed 1 and 3 months after implantation, and the entire portion of the defected femur was removed. The samples were immersed in a 10% buffered formaldehyde solution at room temperature to preserve the tissues.

X-ray radiograph and microcomputed tomography evaluations. After 1 and 3 months of implantation, the right femurs of rabbits were imaged using an X-ray apparatus and were viewed with the Simple View software. Microcomputed tomography (micro-CT) images of the scaffold implants and nonimplants were processed using the Skyscan Desktop Micro-CT 1172 (Arrrselaar) at 60 kV source voltage and 167 μA current, and were used to obtain X-ray radiographs. The scans were reconstructed using the NRecon software and were analyzed with the CTAn software. The Skyscan software was used to calculate the bone volume/tissue volume (BV/TV), bone mineral density (BMD), and total porosity (TP).

Histological observation. The harvested implant samples were fixed in a 10% buffered formaldehyde solution for 1 week and rinsed under tap water for 12 h. After dehydration through a sequential alcohol (70–100%) treatment, the samples were immersed in xylene, paraffin-saturated xylene, and paraffin embedded. The samples were cut to about 5 μm in thickness and were stained with hematoxylin and eosin (H&E) and Masson's trichrome to visualize the cells under an optical microscope (Olympus BX51).

Immunohistochemistry. Immunohistochemistry staining was performed with specific primary antibodies and developed using the Dako REAL™ EnVision kit (K5007), following the manufacturer's instructions. Briefly, sections were subjected to target antigen retrieval with a citrate buffer; blocked with serum for 30 min, and then incubated with the anti-OPN primary antibody (1:100, NB110-89062; Novus Biologicals), anti-OCN (10 μg/mL, ab13418; abcam), and anti-collagen I (1:100, ab90395; abcam) for 1 h. After washing with a wash buffer, samples were incubated with secondary antibodies and Envision/HRP detection for 30 min. Negative controls were prepared by omitting the primary antibody step.

Statistical analysis

All statistical analyses were performed using SPSS (Statistical Package for the Social Sciences, version 16; SPSS, Inc.). Results are expressed as mean ± standard deviation.[25] The Student's *t*-test was used to compare different treatment groups, with significance assigned at $p < 0.05$.

Results

Structural and chemical analyses

The sponge BCP and HyA-Gel hydrogel scaffolds were fabricated using the replica and the freeze-dry methods. The morphologies of the sponge-like BCP architecture, the HyA-Gel hydrogel, and the HyA-Gel/BCP scaffolds were observed by an optical microscope and SEM, as shown in Figure 1. All scaffolds were highly porous with a 3D network of interconnected pore structures. Figure 1A and B show the sponge BCP with interconnected macropores, whose sizes ranged from 50 to 1000 μm, and the struts of the sintered scaffolds were approximately 50–100 μm thick. Figure 1C and D show the cross section of the HyA-Gel hydrogel after freeze drying the lyophilized hydrogel. Unique channelized microstructures were observed. The channels were divided into multiple segments by thin separators that were about 1 μm thick.

The morphology of the porous hybrid HyA-Gel/BCP scaffolds is shown in Figure 1E, F, and H. The porous HyA-Gel hydrogel formed interconnected pore structures between the spaces of the sponge BCP. The images obtained by light microscopy and SEM clearly showed the smaller pores of the HyA-Gel as microscopic pores and the bigger pores as macroscopic pores of the sponge BCP.

The EDS spectrum of the crystals in Figure 1I and J revealed a high concentration of Ca and P at the Ca/P ratio of $\sim 1.56 \pm 0.04$, which was very close to BCP stoichiometry. The XRD measurements were performed to examine the phase analysis of the BCP, HyA-Gel hydrogel, and HyA-Gel hydrogel-loaded sponge BCP, as shown in Figure 1G. BCP alone, and in the composite polymer scaffold, revealed HAp and TCP peaks. The strong peaks of HAp at 25.9, 31.1, 31.8, 39.7, 46.6, 49.4, and 53.0 and the few TCP peaks at 27.8, 32.9, 34.4, and 48.0 are clearly observed in Figure 1G. The characteristic pattern of the HyA-Gel hydrogel exhibited a peak at 19°. This result confirmed the presence of the HyA-Gel hydrogel and sponge BCP in the HyA-Gel/BCP scaffolds.

Macroscopic and microscopic porosity as well as the pore size are important morphological properties of a biomaterial scaffold during bone regeneration. Mercury intrusion porosimetry in Figure 2A demonstrated the porosity distribution and the wide range of pore diameters of sponge BCP, HyA-Gel hydrogel, and HyA-Gel/BCP scaffolds. The porosity was measured as $85.81\% \pm 0.61\%$ for the sponge BCP and $91.49\% \pm 0.53\%$ for the HyA-Gel hydrogel scaffold (Table 1). The HyA-Gel hydrogels had the highest porosity values with the smallest pores. After HyA-Gel loading into the sponge BCP, the porosity of the HyA-Gel/BCP scaffolds increased significantly to 89.27 ± 0.62 compared with that of the sponge BCP, because the HyA-Gel/BCP scaffolds had two types of pores: the pores of the HyA-Gel hydrogel and the pores of the sponge BCP. Figure 2B shows the compressive strength curves of the BCP, HyA-Gel, and HyA-Gel/BCP scaffolds. The compressive strength was determined to be 1.3 ± 0.05, 2.5 ± 0.1, and 2.8 ± 0.15 MPa for BCP, HyA:Gel, and HyA-Gel/BCP scaffolds, respectively. The compressive strength of HyA-Gel/BCP scaffolds was close to that of a cancellous bone.[26] These results show that the network formed by HyA and Gel provided high mechanical strength to the final scaffold. However, the mechanical strength can be controlled by adjusting the composition of the composites for regenerative applications.

In vitro *cytocompatibility*

Proliferation of BMSCs cultured on BCP, HyA-Gel, and HyA-Gel/BCP scaffolds. BMSCs were cultured on the

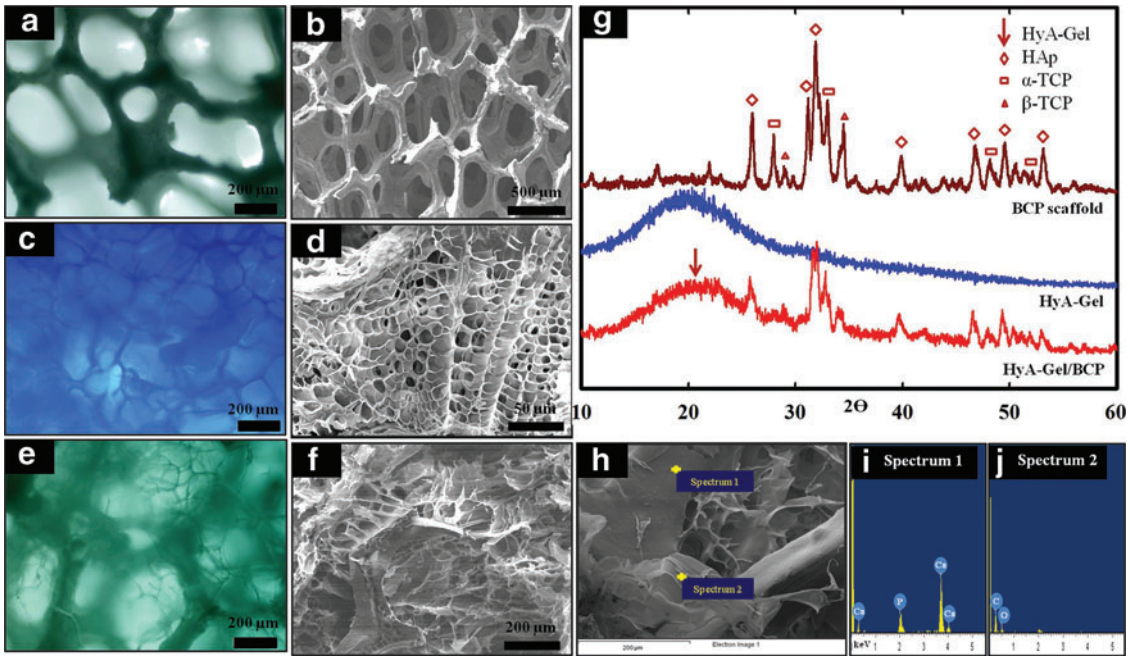

FIG. 1. Morphologies of sponge biphasic calcium phosphate (BCP) scaffold **(a, b)**, hyaluronic acid (HyA)–gel hydrogel **(c, d)**, and HyA-Gel/BCP scaffold **(e, f, h)** observed by a light microscope and SEM showing the high porosity of both scaffolds. XRD **(g)** and EDS profiles of HyA-Gel/BCP **(i, j)**. Color images available online at www.liebertpub.com/tea

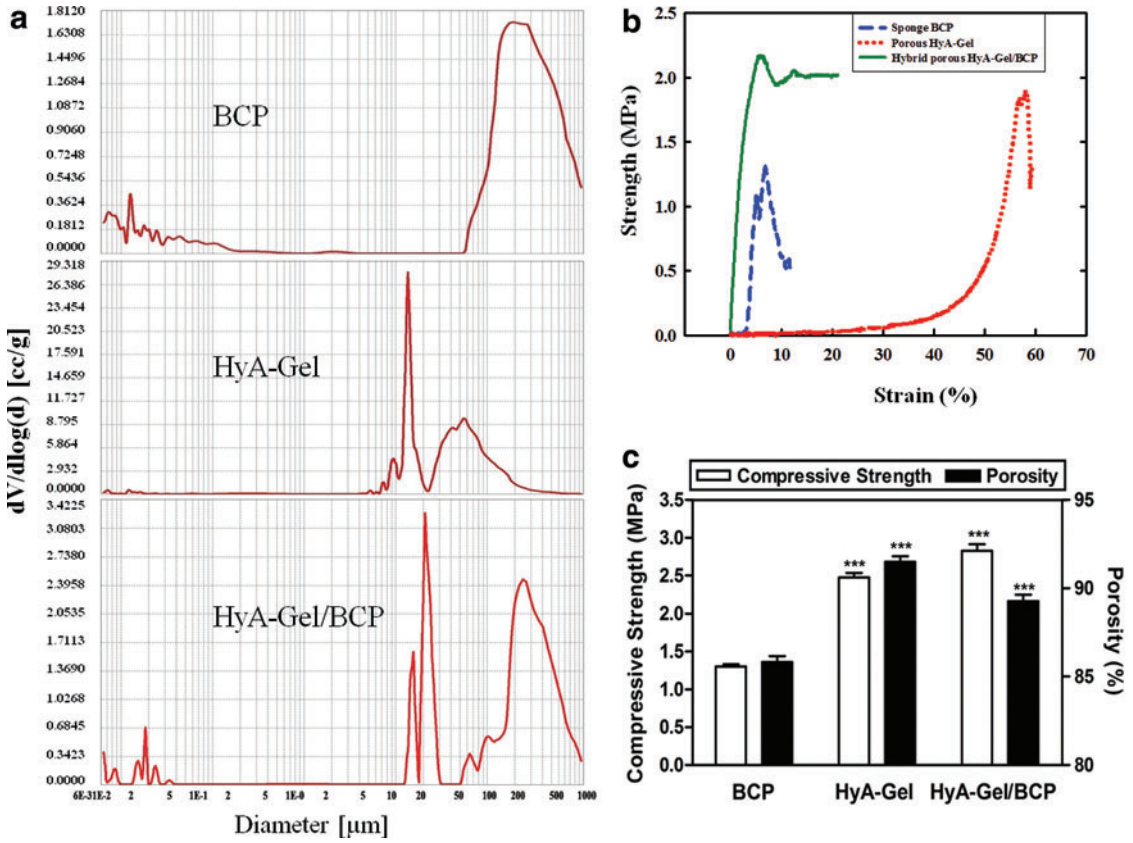

FIG. 2. Mercury intrusion porosimetry demonstrating the pore size distribution and the wide range of pore diameters **(a)**, stress–strain curve **(b)**, and the variations in the porosity and compressive strength of sponge BCP, HyA-Gel hydrogel, and HyA-Gel/BCP **(c)**. ***$p < 0.001$ versus BCP. Color images available online at www.liebertpub.com/tea

TABLE 1. PROPERTIES OF SPONGE BCP, HYA-GEL HYDROGEL, AND HYA-GEL/BCP BEFORE IMPLANTATION

Sample	*Pore size (μm)*	*Porosity*[a] *(%)*	*Compressive strength*[a] *(MPa)*
BCP	200–300	85.81 ± 0.61	1.30 ± 0.05
HyA-Gel	10–20 50–60	91.49 ± 0.53	2.48 ± 0.10
HyA-Gel/BCP	10–20 200–300	89.27 ± 0.62	2.83 ± 0.15

[a]All data are expressed as mean ± standard deviation.
BCP, biphasic calcium phosphate; HYA, hyaluronic acid; Gel, Gelatin.

BCP, HyA-Gel hydrogel, and HyA-Gel/BCP scaffolds to determine whether the HyA-Gel hydrogel loading affected the adhesion and proliferation of BMSCs on the scaffolds. The morphology of the BMSCs is shown in Figure 3a, b, and d. F-actin clearly appeared in BMSC membranes (Fig. 3b) 1 day after seeding on the scaffolds, indicating that the BMSCs were healthy. The confocal images shown in Figure 3a indicate that more cells directly attached to the porous surfaces after 7 days of culture than after 1 and 3 days of culture. Moreover, the BMSCs were well distributed on the scaffolds, indicating that the cells mostly adhered to the microporous hydrogel and grew within the hydrogel in the HyA-Gel hydrogel/BCP system. Cell colonization, both on the surface and in the inner regions of the scaffold, was observed by a confocal microscopy. Confocal observations in Figure 3b show the normal, healthy morphology of the cells, but they were flattened on day 1, indicating adhesion points in the scaffold. The BMSCs continued to grow as the matrices occupied the surfaces of the hydrogel and hydrogel/sponge BCP scaffolds for 3 days and proliferated in between the pores, which were observed on day 7. The cells penetrated into the inner parts of the HyA-Gel hydrogel (Fig. 3b–day 7) and HyA-Gel/BCP (Fig. 3b–day 3 and 7) scaffolds. More cell distribution was observed in the hybrid

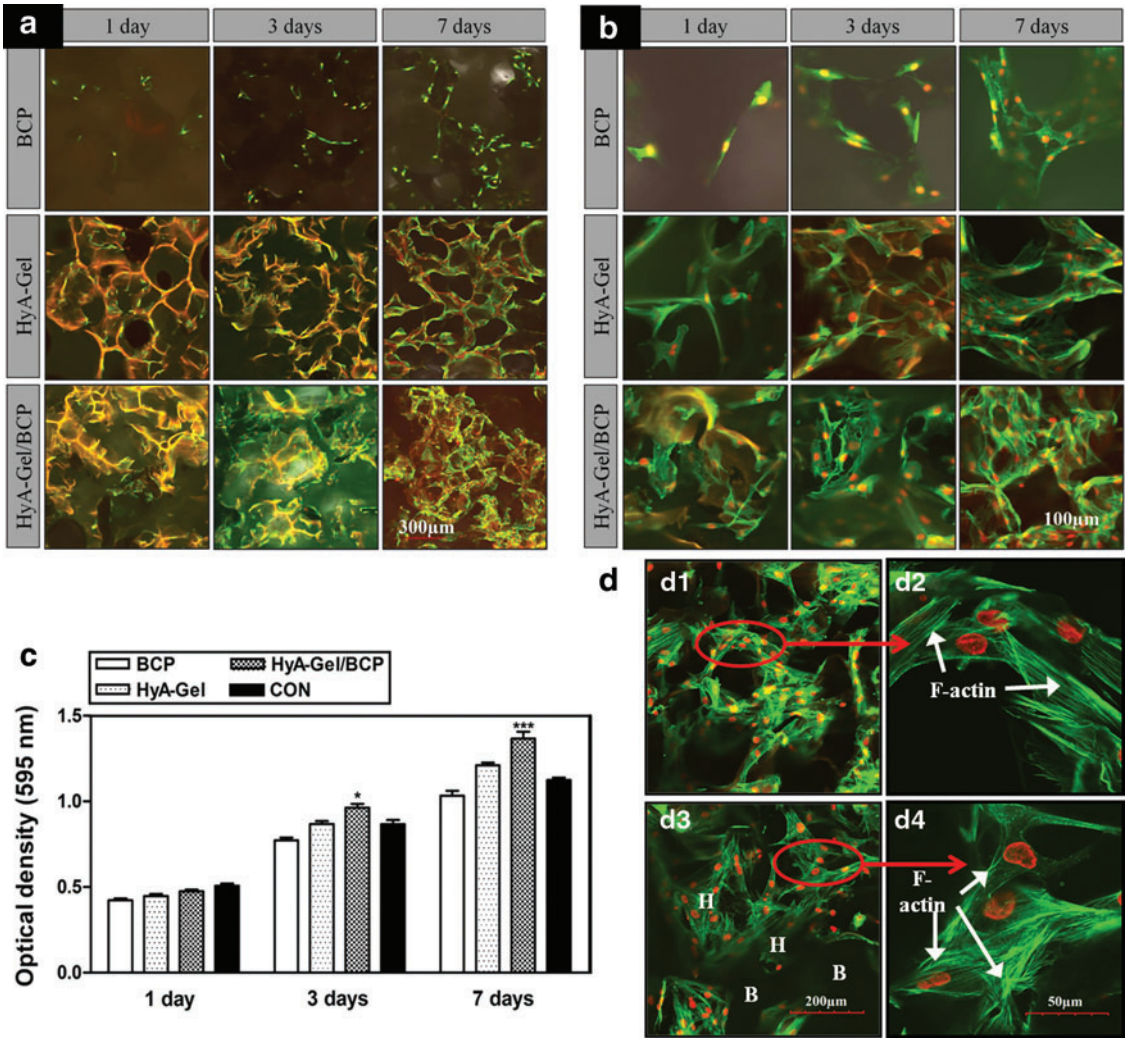

FIG. 3. Effect of porosity on the proliferation of bone marrow mesenchymal stem cells (BMSCs) for sponge BCP, HyA-Gel hydrogel, and HyA-Gel/BCP scaffold after 1, 3, and 7 days of incubation, as observed by a confocal microscope with low magnification **(a)**, high magnification **(b)**, and MTT assay for cell proliferation **(c)**. HyA-Gel/BCP scaffolds showed the highest cell proliferation. $*p < 0.05$, $***p < 0.001$ versus 1 day, **(d)** Filament expression of BMSCs on the HyA-Gel (d1, d2) and HyA-Gel/BCP (H stands for the hydrogel site and B stands for the sponge BCP site) (d3, d4) after 14 days of culture, as observed by a confocal microscope. Color images available online at www.liebertpub.com/tea

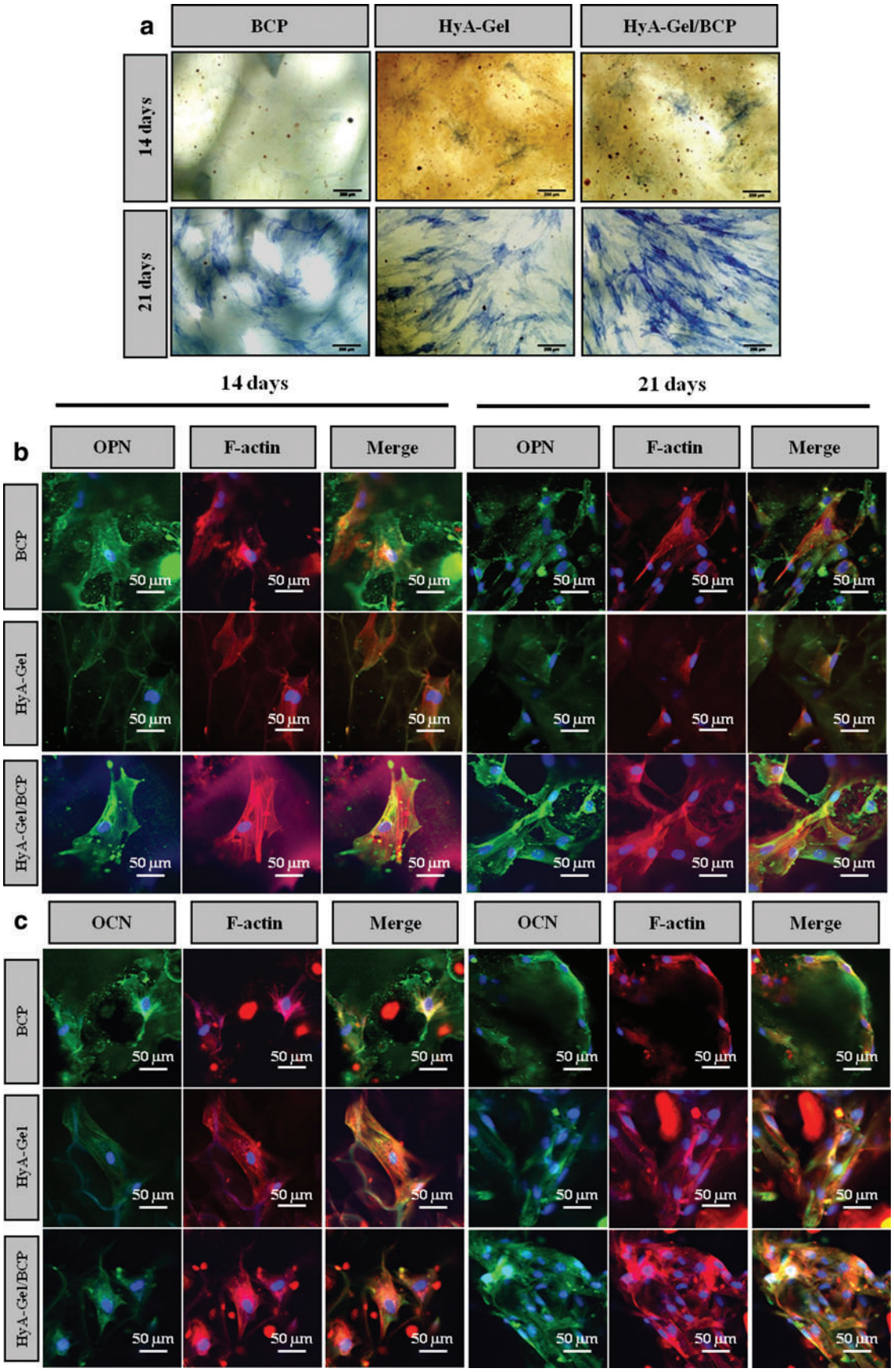

FIG. 4. **(a)** Optical microscope image showing the ALP staining for the differentiation of osteoblasts by BMSCs on 14 and 21 days on BCP, HyA-Gel, and HyA-Gel/BCP scaffolds, immunostaining of cells enabled visualization of protein localization by confocal images with osteopontin (OPN) **(b)** and osteocalcin (OCN) **(c)**. Color images available online at www.liebertpub.com/tea

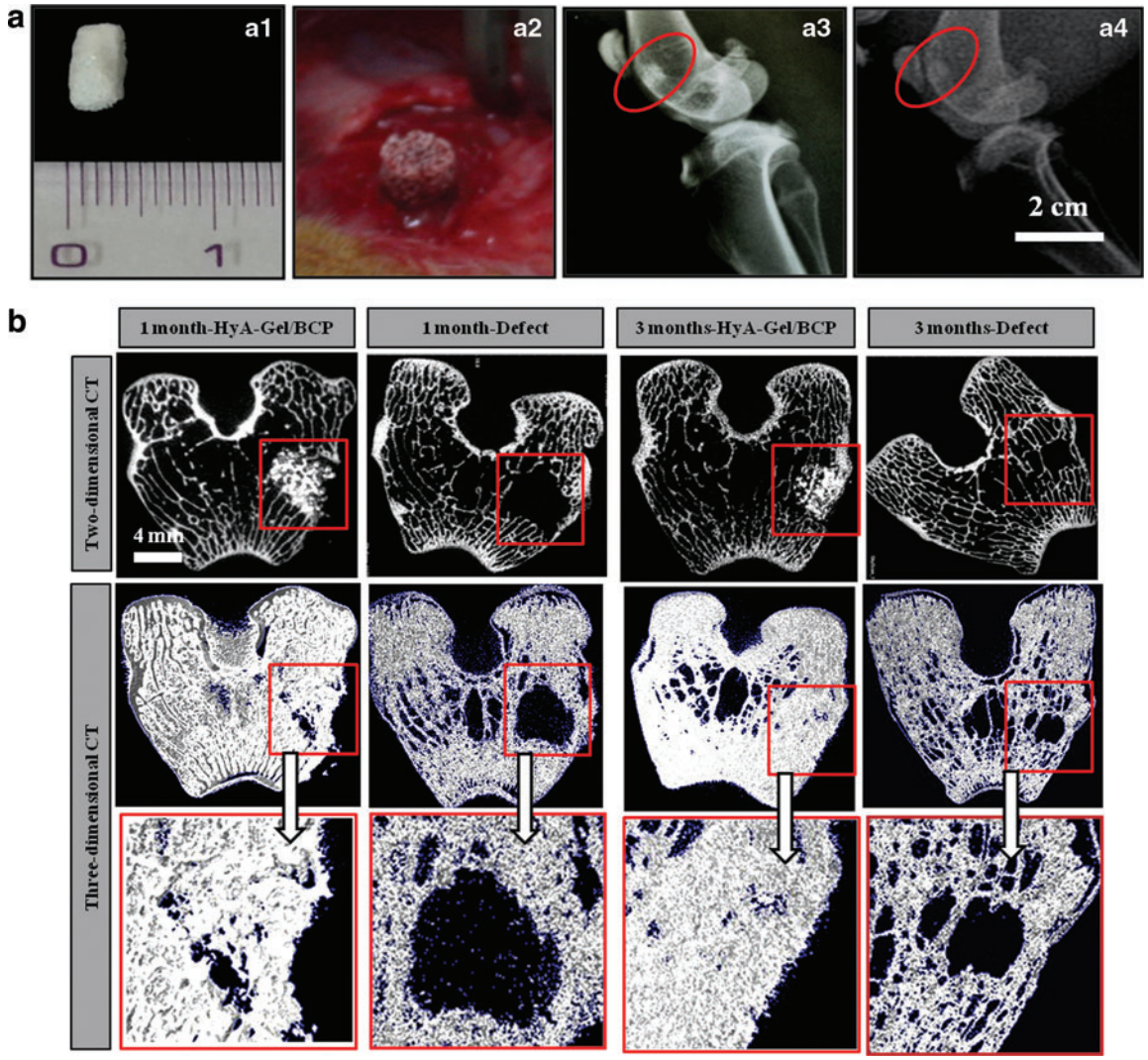

FIG. 5. **(a)** Implantation placement made on a rabbit femur of HyA-Gel/BCP scaffolds (**a1, a2**) after 1 and 3 months. X-ray analysis after 1 (**a3**) and 3 months of implantation (**a4**). The biodegradability of HyA-Gel/BCP was observed after 3 months of implantation. **(b)** Cross-sectional 2D and 3D micro-CT tomograms of the defect (as negative control) and HyA-Gel/BCP scaffolds at 1 and 3 months of implantation. Color images available online at www.liebertpub.com/tea

than that in the other scaffolds. BMSC proliferation on the scaffolds was evaluated using the MTT assay after 1, 3, and 7 days of incubation, as shown in Figure 3c. BMSCs continually proliferated on all the scaffolds from day 1 to 7 in culture, with the highest OD belonging to HyA-Gel/BCP scaffolds.

Growth of BMSCs on the HyA-Gel hydrogel and HyA-Gel/BCP scaffolds was continuously investigated up to 14 days after seeding (Fig. 3d). The cells proliferated along the pore walls of the HyA-Gel hydrogel and HyA-Gel/BCP scaffolds with the appearance of filament actin exhibiting the ability to expand within the scaffolds. On the other hand, the cells spread healthily on both the HyA-Gel hydrogel and HyA-Gel/BCP scaffolds.

Osteogenesis activity. BMSCs were cultured on BCP, HyA-Gel, and HyA-Gel/BCP scaffolds in the osteogenic medium, and the ALP activity was stained as an indication of early-stage bone cell differentiation, as shown in Figure 4a. BMSCs cultured under osteogenic conditions for 2 weeks expressed positive ALP (blue) in the monolayer. We determined a higher ALP activity from HyA-Gel/BCP than from the others at 14 and 21 days. Immunostaining enabled us to visualize protein localization by confocal microscopy, as shown in Figure 4b and c. Primary antibodies against OPN and OCN were applied as bone-specific proteins and relatively late-stage osteogenic differentiation. Both OPN and OCN expressed more intense labeling on the HyA-Gel/BCP scaffolds compared to that on the other scaffolds on days 14 and 21.

Controls in nonosteogenesis on scaffolds were assessed by OPN and OCN immunostaining after 21 days (Supplementary Figure S1; Supplementary Data are available online at www.liebertpub.com/tea). The results showed that the control scaffolds were negative for the OPN and OCN markers.

In vivo *biocompatibility*

X-ray radiograph and micro-CT evaluation. The bone–material scaffold interaction in a living system was investigated by implanting the HyA-Gel/BCP scaffolds in the

TABLE 2. MICRO-CT ANALYSIS OF HYA-GEL/BCP SCAFFOLDS AFTER 1 AND 3 MONTHS OF IMPLANTATION

Groups	*Percent bone volume BV/TV*[a] *(%)*	*Bone mineral density*[a] *(g/cm*^{3}*)*	*Total porosity*[a] *(%)*
1 month	23.97 ± 3.76	0.49 ± 0.02	70.38 ± 1.80
3 months	45.99 ± 1.81	0.72 ± 0.02	55.75 ± 1.47
Native bone	82.84 ± 1.13	0.84 ± 0.02	48.28 ± 1.91

[a]All data are expressed as mean ± standard deviation.
BV/TV, bone volume/tissue volume.

femurs of rabbits for 1 and 3 months. Cylindrical implants of 4 mm in diameter and 5 mm in length were placed into the rabbit femoral bones, following the guidelines in,[27–28] as shown in Figure 5a (a1, a2). The biodegradability of HyA-Gel/BCP was evaluated by X-ray analysis. Figure 5a3 shows the high contrast between the implanted HyA-Gel/BCP scaffold and the natural surrounding bone. The images in Figure 5a4 show a low contrast between the scaffold and the natural bone, indicating the degradation of HyA-Gel/BCP 3 months after implantation.

Micro-CT scanning images in Figure 5b show the integration of the sample and the natural bone tissue, as well as material degradation after 1 month. The morphology of HyA-Gel/BCP was maintained at 1 month; however, degradation of HyA-Gel/BCP scaffolds began to occur 3 months after implantation. Percentage bone volume (BV/TV), BMD, and TP measurements of the newly formed bone are provided in Table 2. The BV/TV of the 3-month group (46 ± 1.8) was greater compared with the 1-month group (24 ± 3.7), but lower compared with the positive control group (left as natural femur bone 83 ± 1.1). Bone loss or low BMD are common in patients with osteoporosis. To identify the causes and the mechanism of osteoporosis, BMD needs to be measured. Table 2 shows that the BMD value after 1 month of implantation (0.49 ± 0.02) was significantly lower compared to that after 3 months of implantation (0.72 ± 0.02).

Histological observations. The evidence of new bone formation and the contact of new bone at the material interface are clearly observed in Figure 6a by histological analyses of HyA-Gel/BCP. New bone was found inside the implant and filled the pores of the scaffolds 1 month after implantation as characterized by the pink color of eosin. At 1 month, the quality of the new bone inside the pores and the quality of the implant perimeter in direct contact with the new bone varied greatly among the samples. New bone formation increased with time. The newly formed bone at 3 months was larger in volume than that at 1 month after implantation. Interestingly, the border between the implanted scaffolds and the native bone became obscure, indicating no inflammation and a high

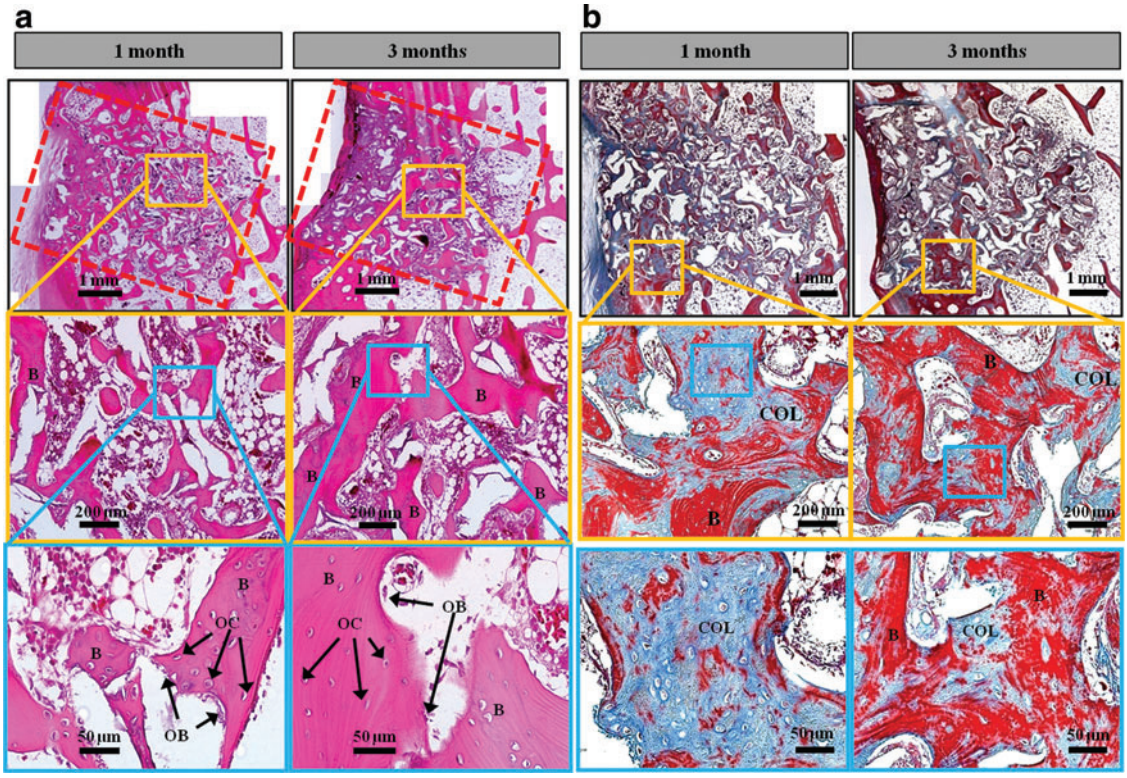

FIG. 6. **(a)** Histological sections of rabbit femur with implanted HyA-Gel/BCP using hematoxylin and eosin staining showing a new bone formation (B), osteocyte (OC) and osteoblast (OB). At month 1, most of the pores were filled with a newly formed bone and the bone formation appeared more clearly with a larger area at month 3. **(b)** Histological sections of rabbit femur with implanted HyA-Gel/BCP using Masson's trichrome staining showing the collagen (COL) deposited within the scaffold site indicated by blue stains and the new bone formation (B) by red stains. Color images available online at www.liebertpub.com/tea

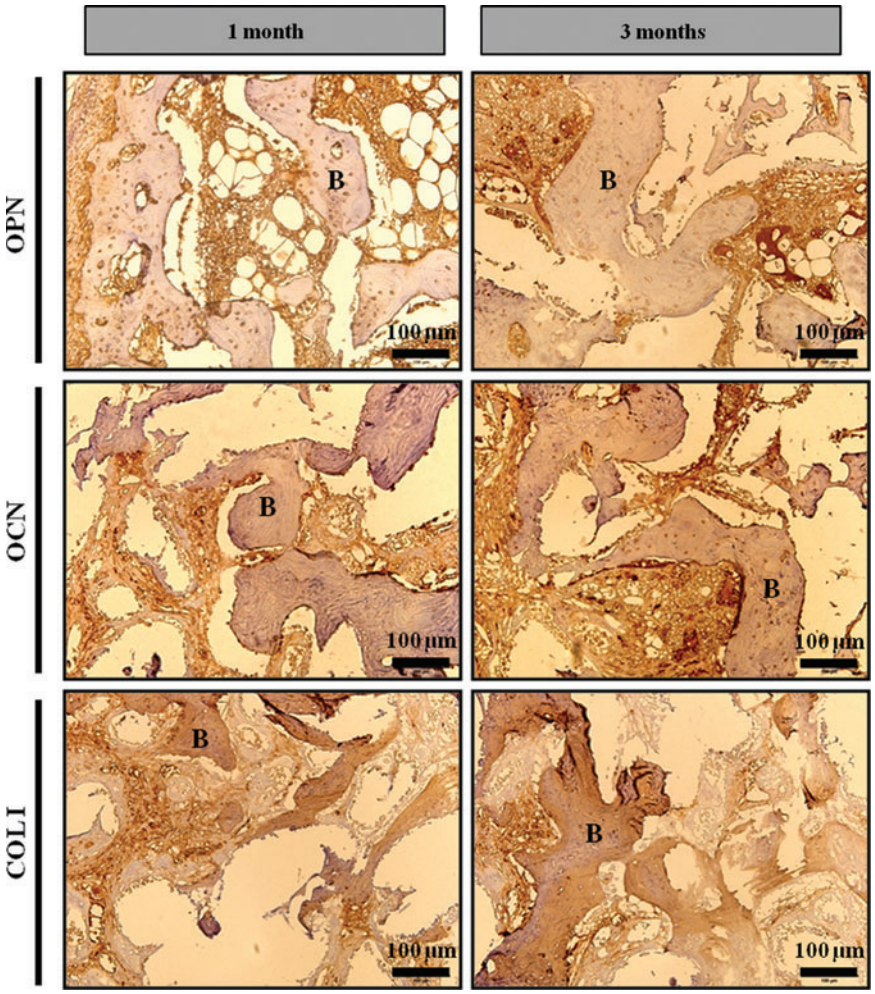

FIG. 7. Deposition of new bone matrix in HyA-Gel/BCP scaffolds after 1 and 3 months of implantation. Bone matrix formation was confirmed by positive immunohistochemistry staining of osteopontin (OPN), osteocalcin (OCN), and collagen type I (COL I). Color images available online at www.liebertpub.com/tea

interconnection between the implanted scaffolds and the native bone.

Masson trichrome stain was used for HyA-Gel/BCP–implanted scaffolds, 1 and 3 months after implantation to confirm the osteoblastic activity. Figure 6b shows the appearance of collagen in the sites of scaffolds (blue stain) and the newly grown bone (red stain) within the scaffolds. Much more collagen was observed at 1 month than at 3 months, while the new bone formation at month 3 was better. The collagen-rich regions were further validation of the biocompatibility of HyA-Gel/BCP scaffolds *in vivo*.

In vivo osteogenesis was evaluated by positive immunohistochemistry staining at the site of the porous HyA-Gel/BCP scaffold implantation after 1 and 3 months. Figure 7 shows the expression of the biomarkers of collagen 1 (COL 1), osteonectin (OCN), and OPN in bone matrix over time. Increased expression of OPN and OCN was observed at 3 months, whereas depression of COL I was evident at the same time.

Discussion

Structures with a high pore density and high degree of interconnectivity among the pores are optimum scaffolds for bone tissue engineering.[29] Therefore, the porosity and pore size of biomaterial scaffolds play a critical role in bone formation both *in vitro* and *in vivo*.[12] In this study, 3D hybrid porous HyA-Gel/BCP scaffolds of well-defined structure, optimum porosity, and high mechanical strength were fabricated by a combined technique of freeze drying and replica process. A new approach was performed by combining the macropore structure of ceramic and the micropore structure of polymers into a hybrid system, which improved compressive strength, had high affinity to the ECM, and provided good biodegradability of the final scaffolds.

The macroscopic system consisted of the sponge BCP, and the microscopic structure was the HyA-Gel hydrogel. Both the macroscopic and microscopic levels are important morphological properties for a biomaterial scaffold to regenerate bone.[5] The pore sizes of the microsponge HyA-Gel hydrogel ranged from 10 to 20 μm and from 50 to 60 μm, which promoted cell adhesion by providing a high specific surface area,[30] and theoretically allowed cell migration or tissue invasion from pore to pore.[31] Such high specific surface areas are also important for protein adhesion and vascularization**.** As tissue formation progresses, the hydrogel matrices are replaced by naturally secreted ECMs from the cells. The pore size of the macrosponge of BCP was 200–300 μm, which provided the framework for bone ingrowths into the pore. In some previous studies, BCP

(hydroxyapatite TCP) scaffolds with 50% porosity and 100–150 μm pore sizes have been shown to aid the recovery of femoral defects in dogs.[32,33] Thus, in the present study, sponge BCP with 80% porosity, a novel composite, can enhance osteointegration as well as reinforce the initial pore structure for bone regeneration.

In general, the sufficient mechanical strength of a scaffold should maintain a suitable matrix for cell ingrowths and nutrient transport *in vitro,* and support physiological loading *in vivo,* and physical strength until the new tissue has formed.[34] Moreover, the scaffolds should provide mechanical support for cells and tissues to infiltrate and grow within the macrostructure. The loaded hydrogel in the sponge BCP scaffold affects the compressive strength, but not the porosity of the HyA-Gel/BCP scaffolds. The compressive strength in Figure 2b and c shows the improved compressive strength of the HyA-Gel/BCP scaffolds after hydrogel loading from that of the sponge BCP. The compressive strength value of HyA-Gel/BCP (2.8 ± 0.15 MPa) was acceptable for cancellous bone implantation.[35] The pore size combination of the HyA-Gel hydrogel and sponge BCP, resulting in various pore sizes of the HyA-Gel/BCP system, improved the compressive strength of the HyA-Gel/BCP scaffolds.

Cell growth within the porous scaffolds is critical for tissue reconstruction.[36] Thus, biological responses of osteoblast cells in the fabricated bone substitute, such as cell adhesion behavior and proliferation ability were investigated. Results in Figure 3 show the increasing growth rate of the cells with time. The advantage of a 3D structure over flat surfaces is that it can introduce sufficient space for cell growth and reproduction. In relation to the porous network of the fabricated scaffold, porosity is also important in that, it aids nutrient exchange and diffusion across the material and, therefore, provides an optimum environment for cell proliferation. Confocal microscopy revealed the ability of the cells to attach to the 3D constructs. A closer observation of the attachment and extension of BMSCs on the scaffolds is shown in Figure 3d. The appearance of actin staining with FITC-conjugated phalloidin[37] indicated the health status of the cells from day 1 to 7 of culture. The cells fully covered the scaffolds with good cell–matrix interactions on day 14 of culture. The cells proliferated along the pore wall of the scaffolds, similar to the process of bone remodeling. Additionally, the location of microfilaments, composed of actin filaments in cell membranes, could be distinguished in the multiple structures of the same cell; thus, the relative orientations of the HyA-Gel hydrogel and HyA-Gel/BCP scaffolds could be compared.

Due to the short developmental period, New Zealand white rabbits were selected to determine the *in vivo* biocompatibility of HyA-Gel/BCP scaffolds.[38] The implanted scaffolds, observed by X-ray, did not biodegrade by the end of the first month, but started to degrade at 3 months, although not to completion. The micro-CT technique demonstrated significant bone formation during 1 and 3 months. BV/TV increased with implantation time, indicating that the scaffolds responded well to cancellous bone. The histological study showed the bone repair characteristics of the rabbit femur. Histology was used to evaluate osteogenesis and the degradation of HyA-Gel/BCP. Porous BCP has been highlighted for its biocompatibility and osteoconductive architecture. After 1 month of implantation, extensive bone volume was detected not only on the pore surfaces, but also in the center of the pores of the implants. Vasculature formed and osteoblast growth was observed in the porous microstructure, and the implanted artificial bone gradually replaced the scaffold, the results of which showed the potential of the implant for natural bone replacement. Bone tissue formation became more apparent after 3 months, and the scaffold-implanted femurs exhibited a higher bone volume compared with the1-month group relative to the scaffold pores, indicating that the kinetics of bone repair is dependent on the implantation time. The subsequent formation of blood vessels was also observed, suggesting vasculature development in the area. Additionally, the excellent integration of the scaffold and native bone was observed without any sign of inflammation. In this study, three biomarkers for osteogenesis were assayed using immunohistochemistry to evaluate *in vivo* osteogenesis. At 1- and 3-month periods, expression of collagen 1 (COL I), OCN, and OPN was found at the site of bone matrix of implanted HyA-Gel/BCP scaffolds (Fig. 7). Although OPN and OCN increased over time, COL I expression decreased. Decreased COL I was also observed by the Masson's trichrome study (Fig. 6b). The reason for decreased collagen I expression was obvious due to early-stage expression of collagen during osteogenesis.[39,40]

Conclusions

A novel system of loading the ''HyA-Gel'' hydrogel into a sponge BCP scaffold to fabricate a hybrid scaffold for bone tissue engineering was discussed in this study. An intelligent architectural orientation of porosity was introduced so that the microsponge HyA-Gel combined with macrosponge BCP. As a result, such a combination greatly provided favorable cellular homing as well enhanced mechanical strength to support the initial load of bearing necessary for cancellous bones. Our evaluative *in vitro* and *in vivo* studies clearly exhibited cellular proliferation and bone accelerated regeneration due to such novel designing of the scaffold system. The combination of sponge BCP and HyA-Gel hydrogel facilitated the bone-bonding activity of the material to the native bone tissue as it was observed by histological analysis in the rabbit femur after implantation. *In vivo* osteogenesis was also evidenced through immunohistochemical analysis, which showed an excellent corelation with cell proliferation, tissue regeneration, and other published data. Thus, preclinical studies confirmed the usefulness of HyA-Gel/BCP scaffolds. However, further studies will be necessary at a clinical setup to evaluate the efficacy of the scaffold to heal the patient. We believe that the HyA-Gel/BCP model reflects that the newly developed material is an excellent scaffold for bone remodeling. The components of the hydrogel or sponge scaffolds can be adjusted when necessary for use with scaffolds in other *in vivo* osteogenesis applications.

Acknowledgments

This work was supported by the Mid-career Research Program (NRF), grant number 2009-0092808, the Republic of Korea and partially supported by Soonchunhyang University Research Fund. The authors would like to thank Mr. Shin Woo Kim for the contribution of *in vivo* operations.

Disclosure Statement

No competing financial interests exist.

References

1. Langer, R., and Vacanti, J.P. Tissue engineering. Science **260,** 920, 1993.
2. Liu, X., and Ma, P.X. Polymeric scaffolds for bone tissue engineering. Ann Biomed Eng **32,** 477, 2004.
3. Molly, M.S. Biomaterials for bone tissue engineering. Mater Today **11,** 18, 2008.
4. Shin, H., Jo, S., and Mikos, A.G. Biomimetic materials for tissue engineering. Biomaterials **24,** 4353, 2003.
5. Yang, S., Leong, K.-F., Du, Z., and Chua, C.-K. The design of scaffolds for use in tissue engineering. Part I. Traditional factors. Tissue Eng **7,** 679, 2001.
6. Cao, H., and Kuboyama, N. A biodegradable porous composite scaffold of PGA/[beta]-TCP for bone tissue engineering. Bone **46,** 386, 2010.
7. Sun, L., Wu, L., Bao, C., Fu, C., Wang, X., Yao, J., Zhang, X., and van Blitterswijk, C.A. Gene expressions of Collagen type I, ALP and BMP-4 in osteo-inductive BCP implants show similar pattern to that of natural healing bones. Mater Sci Eng **C 29,** 1829, 2009.
8. Fellah, B.H., Gauthier, O., Weiss, P., Chappard, D., and Layrolle, P. Osteogenicity of biphasic calcium phosphate ceramics and bone autograft in a goat model. Biomaterials **29,** 1177, 2008.
9. Slaughter, B.V., Khurshid, S.S., Fisher, O.Z., Khademhosseini, A., and Peppas, N.A. Hydrogels in regenerative medicine. Adv Mater **21,** 3307, 2009.
10. Weigel, P.H., Hascal, V.C., and Tammi, M. Hyaluronan synthases. J Biol Chem **272,** 13997, 1997.
11. Tan, H., Gong, Y., Lao, L., Mao, Z., and Gao, C. Gelatin/chitosan/hyaluronan ternary complex scaffold containing basic fibroblast growth factor for cartilage tissue engineering. J Mater Sci Mater Med **18,** 1961, 2007.
12. Karageorgiou, V., and Kaplan, D. Porosity of 3D biomaterial scaffolds and osteogenesis. Biomaterials **26,** 5474, 2005.
13. Chang, C.-H., Liu, H.-C., Lin, C.-C., Chou, C.-H., and Lin, F.-H. Gelatin-chondroitin-hyaluronan tri-copolymer scaffold for cartilage tissue engineering. Biomaterials **24,** 4853, 2003.
14. Farris, S., Schaich, K.M., Liu, L., Cooke, P.H., Piergiovanni, L., and Yam, K.L. Gelatin-pectin composite films from polyion-complex hydrogels. Food Hydrocolloids **25,** 61, 2011.
15. Linh, N.T.B., and Lee, B.-T. Electrospinning of polyvinyl alcohol/gelatin nanofiber composites and cross-linking for bone tissue engineering application. J Biomater Appl **27,** 255, 2012.
16. Zhang, Y., Ouyang, H., Lim, C.T., Ramakrishna, S., and Huang, Z.-M. Electrospinning of gelatin fibers and gelatin/PCL composite fibrous scaffolds. J Biomed Mater Res Part B **72B,** 156, 2005.
17. Pal, K., Banthia, A., and Majumdar, D. Preparation and characterization of polyvinyl alcohol-gelatin hydrogel membranes for biomedical applications. AAPS PharmSciTech **8,** E142, 2007.
18. Linh, N.T.B., Min, Y., and Lee, B.-T. Fabrication and *in vitro* evaluations with osteoblast-like MG-63 cells of porous hyaluronic acid-gelatin blend scaffold for bone tissue engineering applications. J Mater Sci **48,** 4233, 2013.
19. Kim, M., Franco, R.A., and Lee, B.-T. Synthesis of functional gradient BCP/ZrO2 bone substitutes using ZrO2 and BCP nanopowders. J Eur Ceram Soc **31,** 1541, 2011.
20. Park, S.-H., Sim, W.Y., Park, S.W., Yang, S.S., Choi, B.H., Park, S.R., Park, K., and Min, B.-H. An electromagnetic compressive force by cell exciter stimulates chondrogenic differentiation of bone marrow–derived mesenchymal stem cells. Tissue Eng **12,** 3107, 2006.
21. Cui, J.H., Park, K., Park, S.R., and Min, B.-H. Effects of low-intensity ultrasound on chondrogenic differentiation of mesenchymal stem cells embedded in polyglycolic acid: an in vivo study. Tissue Eng **12,** 75, 2006.
22. Alhadlaq, A., and Mao, J.J. Mesenchymal stem cells: isolation and therapeutics. Stem Cells Dev **13,** 436, 2004.
23. Mickisch, G., Fajta, S., Keilhauer, G., Schlick, E., Tschada, R., and Alken, P. Chemosensitivity testing of primary human renal cell carcinoma by a tetrazolium based microculture assay (MTT). Urol Res **18,** 131, 1990.
24. Story, B., Wagner, W., Gaisser, D., Cook, S., and Rust-Dawicki, A. *In vivo* performance of a modified CSTi dental implant coating. Int J Oral Maxillofac Implants **13,** 749, 1998.
25. Leong, K.F., Chua, C.K., Sudarmadji, N., and Yeong, W.Y. Engineering functionally graded tissue engineering scaffolds. J Mech Behav Biomed Mater **1,** 140, 2008.
26. Pearce, A.I., Richards, R.G., Milz, S., Schneider, E., and Pearce, S.G. Animal models for implant biomaterial research in bone: a review. Eur Cells Mater **13,** 1, 2007.
27. 10993–6. 1994. International Standard ISO Biological evaluation of medical devices. Part 6: Test for local effects after implantation, pages 1–11
28. Chan, K.S., Liang, W., Francis, W.L., and Nicolella, D.P. A multiscale modeling approach to scaffold design and property prediction. J Mech Behav Biomed Mater **3,** 584, 2010.
29. Cima, L.G., Vacanti, J.P., Vacanti, C., Ingber, D., Mooney, D., and Langer, R. Tissue engineering by cell transplantation using degradable polymer substrates. J Biomech Eng **113,** 143, 1991.
30. Steinkamp, J.A., Hansen, K.M., and Crissman, H.A. Flow microfluorometric and light-scatter measurement of nuclear and cytoplasmic size in mammalian cells. J Histochem Cytochem **24,** 292, 1976.
31. Cong, Z., Jianxin, W., Huaizhi, F., Bing, L., and Xingdong, Z. Repairing segmental bone defects with living porous ceramic cylinders: An experimental study in dog femora. J Biomed Mater Res **55,** 28, 2001.
32. Zhang, C., Wang, J., Feng, H., Lu, B., Song, Z., and Zhang, X. Replacement of segmental bone defects using porous bioceramic cylinders: A biomechanical and X-ray diffraction study. J Biomed Mater Res **54,** 407, 2001.
33. Leong, K.F., Cheah, C.M., and Chua, C.K. Solid freeform fabrication of three-dimensional scaffolds for engineering replacement tissues and organs. Biomaterials **24,** 2363, 2003.
34. Martin, R.B., Chapman, M.W., Sharkey, N.A., Zissimos, S.L., Bay, B., and Shors, E.G. Bone ingrowth and mechanical properties of coralline hydroxyapatite 1 yr after implantation. Biomaterials **14,** 341, 1993.
35. Zhen, W., Jiang, C., Feng, B., Xiaojiang, S., Jianxi, L., Li, L., Chen, L., and Rong, D. Role of the porous structure of the bioceramic scaffolds in bone tissue engineering. Nat Precedings 2010. http://hdl.handle.net/10101/npre.2010.4148.1.
36. Green, D., Walsh, D., Mann, S., and Oreffo, R.O.C. The potential of biomimesis in bone tissue engineering: lessons

from the design and synthesis of invertebrate skeletons. Bone **30,** 810, 2002.
37. Gilsanz, V., Roe, T.F., Gibbens, D.T., Schulz, E.E., Carlson, M.E., Gonzalez, O., and Boechat, M.I. Effect of sex steroids on peak bone density of growing rabbits. Am J Physiol **255,** E416, 1988.
38. Hoshiba, T., Kawazoe, N., Tateishi, T., and Chen, G. Development of stepwise osteogenesis-mimicking matrices for the regulation of mesenchymal stem cell functions. J Biol Chem **284,** 31164, 2009.
39. Polini, A., Pisignano, D., Parodi, M., Quarto, R., and Scaglione, S. Osteoinduction of human mesenchymal stem cells by bioactive composite scaffolds without supplementary osteogenic growth factors. PLoS One **6,** e26211, 2011.

Address correspondence to:
Byong-Taek Lee, PhD
Department of Regenerative Medicine
College of Medicine
Soonchunhyang University
366-1 Ssangyong dong
Cheonan 330-090
South Korea

E-mail: lbt@sch.ac.kr

Received: June 12, 2013
Accepted: January 29, 2014
Online Publication Date: March 19, 2014